doi:10.1006/jmbi.2001.5195 available online at http://www.idealibrary.com on IDEAL® J. Mol. Biol. (2001) 314, 823–837

JMB

Refined Crystallographic Structure of *Pseudomonas aeruginosa* Exotoxin A and its Implications for the Molecular Mechanism of Toxicity

Joseph E. Wedekind[1], Christine B. Trame[1], Magdalena Dorywalska[1] Patrice Koehl[1], Tanya M. Raschke[1], Marian McKee[2], David FitzGerald[2] R. John Collier[3] and David B. McKay[1]*

[1]*Department of Structural Biology, Stanford University School of Medicine, Stanford CA 94305, USA*

[2]*Laboratory of Molecular Biology, Division of Cancer Biology, National Cancer Institute, National Institutes of Health, Bethesda MD 20892, USA*

[3]*Department of Microbiology and Molecular Genetics Harvard Medical School Boston, MA 02115, USA*

**Corresponding author*

Exotoxin A of *Pseudomonas aeruginosa* asserts its cellular toxicity through ADP-ribosylation of translation elongation factor 2, predicated on binding to specific cell surface receptors and intracellular trafficking *via* a complex pathway that ultimately results in translocation of an enzymatic activity into the cytoplasm. In early work, the crystallographic structure of exotoxin A was determined to 3.0 Å resolution, revealing a tertiary fold having three distinct structural domains; subsequent work has shown that the domains are individually responsible for the receptor binding (domain I), transmembrane targeting (domain II), and ADP-ribosyl transferase (domain III) activities, respectively. Here, we report the structures of wild-type and W281A mutant toxin proteins at pH 8.0, refined with data to 1.62 Å and 1.45 Å resolution, respectively. The refined models clarify several ionic interactions within structural domains I and II that may modulate an obligatory conformational change that is induced by low pH. Proteolytic cleavage by furin is also obligatory for toxicity; the W281A mutant protein is substantially more susceptible to cleavage than the wild-type toxin. The tertiary structures of the furin cleavage sites of the wild-type and W281 mutant toxins are similar; however, the mutant toxin has significantly higher *B*-factors around the cleavage site, suggesting that the greater susceptibility to furin cleavage is due to increased local disorder/flexibility at the site, rather than to differences in static tertiary structure. Comparison of the refined structures of full-length toxin, which lacks ADP-ribosyl transferase activity, to that of the enzymatic domain alone reveals a salt bridge between Arg467 of the catalytic domain and Glu348 of domain II that restrains the substrate binding cleft in a conformation that precludes NAD^+ binding. The refined structures of exotoxin A provide precise models for the design and interpretation of further studies of the mechanism of intoxication.

Keywords: exotoxin; *Pseudomonas aeruginosa* toxicity; crystal structure; furin; pH-induced conformational change

Introduction

Exotoxin A of *Pseudomonas aeruginosa* (PE)[1] is a virulence factor secreted in response to environmental iron scarcity.[2] The mature protein has 613 amino acid residues and four disulfide linkages. PE is highly toxic to eukaryotic cells, causing the arrest of protein synthesis. This is accomplished

Present address; J. E. Wedekind, Department of Biochemistry and Molecular Biology, The Chicago Medical School, North Chicago, IL 60064, USA.

Abbreviations used: PE, *Pseudomonas aeruginosa* exotoxin A; ER, endoplasmic reticulum; PEG, polyethylene glycol; CCD, charge-coupled device; SSRL, the Stanford Synchrotron Radiation Laboratory; α_{calc}, calculated phases; eEF-2, eukaryotic elongation factor 2; DT, diphtheria toxin.

E-mail address of the corresponding author: Dave.McKay@Stanford.edu

0022-2836/01/040823–15 $35.00/0

through enzymatic ADP-ribosylation of a specific post-translationally modified histidine of eEF-2 (diphthamide).[3–5] At a minimum, presentation of the enzymatic activity of PE in the cytoplasm of target cells requires: (i) cell surface receptor binding and internalization; (ii) proteolytic hydrolysis between Arg279 and Gly280; (iii) reduction of the Cys265-Cys287 disulfide; and (iv) transmembrane translocation of the catalytic domain into the cytoplasmic compartment. Contemporary models for the pathway of intoxication envisage that PE first binds the α_2-macroglobulin receptor and is internalized into endosomes.[6] Then, the toxin is cleaved by the protease furin.[7,8] *In vitro*, furin cleavage occurs only at low pH (typically 5.5 in published assays).[7,9] *In vivo* the cleavage is relatively inefficient, and is believed to occur in endosomes, where the low pH environment induces a conformational change that makes the toxin furin-susceptible.[9,10] Once cut, the toxin is shuttled to the endoplasmic reticulum (ER) and, predicated on the carboxy-terminal lysine having been removed (possibly by a plasma variant of carboxypeptidase early in the intoxication process[11]), is retained there by the carboxy-terminal REDL sequence, which mimics a ER retention signal and binds the KDEL receptor.[12] Subsequently, the furin-generated 37 kDa carboxy-terminal fragment of PE, which includes the enzymatic domain, is translocated into the cytoplasm. The 37 kDa fragment may masquerade as an unfolded/misfolded protein that is exported from the ER through the retrograde protein translocation system;[13,14] an obligatory step in this process is partial unfolding of the furin-nicked PE molecule and reduction of the Cys265-Cys287 disulfide by cellular factors.[15] In the cytoplasm, the enzymatic domain circumvents degradation by the proteasome long enough to enzymatically ADP-ribosylate eEF-2, thereby inhibiting protein synthesis.

The crystallographic structure of native wild-type PE was determined to 3.0 Å resolution several years ago,[16] before efficient methodologies for high-resolution X-ray data collection and protein model refinement were available. Although the model was relatively imprecise by contemporary standards, it revealed the overall tertiary structure of the molecule, which consists of three domains. Domain I (residues 1-252, called Ia; and 365-404, called Ib) has a core formed of a 13-stranded β-roll; domain II (residues 253-364) is a bundle of six α-helices; and domain III (residues 405-613), the enzymatic domain, has a complex α/β-folding topology, distinct from classical nucleotide binding motifs. It was suggested, based on the modular domain structure of the toxin, that domain I was responsible for receptor binding, domain II was required for transmembrane targeting (although the mechanism by which this occurs remains unclear), and domain III was the ADP-ribosyl transferase; these hypotheses have been confirmed by subsequent experiments.[17,18] Knowledge of the tripartite domain structure of PE has been exploited extensively in the construction of chimeric toxins that target specific cell types through replacement of domain Ia with a cytokine or a monoclonal antibody fragment.[19]

Structures of several other bacterial ADP-ribosylating exotoxins have been solved in recent years. The structure of the isolated enzymatic domain III of PA has been solved to 2.3 Å resolution, revealing a conformational change in a flexible loop of the substrate binding cleft which allows substrates to bind in a catalytically productive manner when the domain is untethered from the rest of the molecule.[20,21] Diphtheria toxin (DT) has a three-domain organization, reminiscent of PE, although the catalytic domain is amino-terminal rather than carboxy-terminal.[22] DT ADP-ribosylates eEF-2, with a target specificity identical to that of PE. The heat-labile toxin (LT) from *Escherichia coli*, a close homolog of cholera toxin, has an AB_5 quaternary structure,[23] where the pentameric B subunits bind gangliosides, and the A subunit is the enzymatic domain. Its intracellular target is the Gs_α protein, which stimulates adenylate cyclase. Similarly, the pertussis toxin (PT) is composed of an enzymatic domain and a pentameric receptor binding oligomer constructed from four heteroprotomers (with two copies of one protomer and one copy of each of the other three).[24] The catalytic domain of PT ADP-ribosylates Gi_α, an inhibitor of adenylate cyclase, as well as transducin. Despite negligible sequence similarity between members of this group of toxins, their catalytic ADP-ribosyl transferase domains have a similar tertiary fold.[23,24] This ''ADP-ribosyl transferase'' fold has been found in the enzymatic VP2 domain of a *Bacillus cereus* insecticidal toxin,[25] as well as in the core of vertebrate poly(ADP ribose) polymerase.[26] Hence domain III of PE appears to be a topologically unique fold that is conserved for the specific activity of transferring the ADP-ribosyl moiety of NAD^+ to a spectrum of cellular targets.

Although the structures of the catalytic domains of these toxins are similar, the proteins are more diverse in the routes they employ to gain access to the cytoplasm and the mechanisms by which they activate their enzymatic domains. The enzymatic domain of DT is thought to translocate directly from the endosome into the cytoplasm.[27,28] In contrast, PT,[29] LT and cholera toxin,[30] and PE[12,31] are distinguished by the utilization of a more circuitous route through the ER and the protein retrograde transport system. Despite success in elucidating the pathway by which the catalytic activity of PE reaches the cell cytoplasm, as well as advances in utilizing chimeric toxins as therapeutic agents, questions still remain regarding the molecular mechanisms of several steps in the PE intoxication scheme, including receptor binding, pH-dependent activation, and transmembrane targeting. Accurate molecular models of wild-type PE and mutants with altered function will facilitate the design and interpretation of experiments delineating the mechanisms of these activities at the

molecular level. In this context, we have established conditions that allow high-resolution data collection on PE crystals, and have collected data and refined the structures of wild-type PE (natural toxin produced by *P. aeruginosa*[32]) and a W281A mutant with enhanced susceptibility to furin cleavage but decreased cellular toxicity (recombinant protein from *E. coli*[33]) to 1.62 Å and 1.45 Å resolution, respectively. The PE proteins in this crystal form (and by implication, the molecular models) represent the extracellular state of the toxin, before it has undergone endocytosis and proteolytic processing. As such, the PE structures represent ''snapshots'' of the protein before it progresses through a series of complex biochemical activities that ultimately culminate in cellular intoxication. Here, we present the structures and discuss their relationship to the activities of the toxin.

Results and Discussion

Quality and comparison of the refined models

Both the wild-type and W281A mutant PE models are well defined, with average *B* values of 29.5 Å^2 and 21.9 Å^2, respectively. Crystals of the mutant protein yielded data to somewhat higher resolution due to lower overall mosaicity (0.18° *versus* ~0.6° for wild-type), which can probably be ascribed to improvement in the method of cryoprotection, rather than any intrinsic difference in the two proteins. Several segments of polypeptide on the surfaces of the molecules are poorly ordered, and in the final stages of refinement, interpretation was aided by cross-checking the conformations between the two structures and using the better-ordered representative as a guide for the more poorly ordered. In the end, two segments of polypeptide could not be interpreted: residues 179-184 in domain I, and residues 607-613 at the carboxy terminus. Residues 488-491 are the most poorly ordered segment of polypeptide in the wild-type structure, with *B*-factors in the range 75-88 Å^2; the model of this segment reveals little more than the average path of the polypeptide backbone in this region.

The average coordinate error estimated from a cross-validated Luzzati plot[34,35] is 0.20 Å for the wild-type structure, 0.18 Å for the mutant. A further indication of the model quality can be seen in representative $2F_o - F_c$ and anomalous difference Fourier maps, which reveal monovalent ion binding sites in the crystals (Figure 1). The best-occupied site occurs between the surface guanidinium groups of Arg154 and Arg505′ (Figure 1(a); the prime designates a symmetry-related molecule) at a crystal lattice interface. A less distinct solvent peak near the amino-terminal end of an α-helix in domain III has been assigned as a second Cl ion as well, due to its anomalous signal. This ion does not appear to serve any structural function, but may coordinate due to the solvent accessibility of the backbone amides at residues Asp589 and Lys590 where the ion is afforded a favorable helix dipole interaction. A sodium ion is observed to mediate a second lattice packing contact between the crystallographically related carbonyl oxygen atoms of Asn62 and Pro598′ (Figure 1(b)). Although this atom has no detectable anomalous signal†, its pentacoordinate geometry and close ligand distances of 2.4 Å[36] are consistent with Na^+. The protein carbonyl oxygen atoms contribute axial and equatorial ligands of a trigonal bipyramid, similar to that seen in the Na^+ structure of dialkylglycine decarboxylase,[37] with H_2O molecules contributing the other ligands. High ionic strength (>1.0 M NaCl) is required for crystallization of PE. The interactions of monovalent ions with the toxin that we observe in the presence of 1.0 M NaCl are probably due to low-affinity binding sites and are unlikely to be significant for toxin activity under *in vivo* conditions.

The average rms displacement between the C^α atoms of the refined wild-type model *versus* those of the model reported by Allured *et al.*[16] is 0.58 Å, confirming the original polypeptide trace. The average rms difference in backbone atomic positions between wild-type and the W281A mutant structures is 0.60 Å. When backbone atoms of individual domains are superimposed, the average rms differences are 0.28 Å, 0.32 Å and 0.84 Å for domains I, II and III, respectively; when polypeptide segments that differ substantially in conformation are omitted in domain III, the value is reduced from 0.84 Å to 0.37 Å.

The interface between domains suggests residues that may control the low pH-induced conformational change

The three-domain architecture of PE is illustrated in Figure 2. The last six carboxy-terminal residues cannot be modeled, due to disorder; they presumably distend from domain III so that the penultimate REDL residues are accessible to the KDEL receptor in the endoplasmic reticulum. The furin cleavage site (between Arg279 and Gly280; highlighted with an arrow in Figure 2(c)) is in a surface loop between helices of domain II. However, despite its apparent surface presentation in the PE structure, the site is not accessible to furin at neutral pH; a low pH-induced conformational change is required to allow this peptide segment to become protease-susceptible.[7]

In vitro biophysical studies have demonstrated a conformational transition in PE in the pH range 3.7-5.4;[38] the molecular details of this transition, whether it is a localized perturbation of the furin cleavage site, or a more global ''dissociation'' of domain II from domain I, have not been deter-

† The value of f'' for Cl^- is 0.70 electron at the wavelength of CuK_α radiation ($\lambda = 1.54$ Å), whereas f'' for Na^+ is 0.12 electron.[1] The anomalous contribution to the scattering intensities was measured in-house using a rotating anode X-ray generator with a copper target.

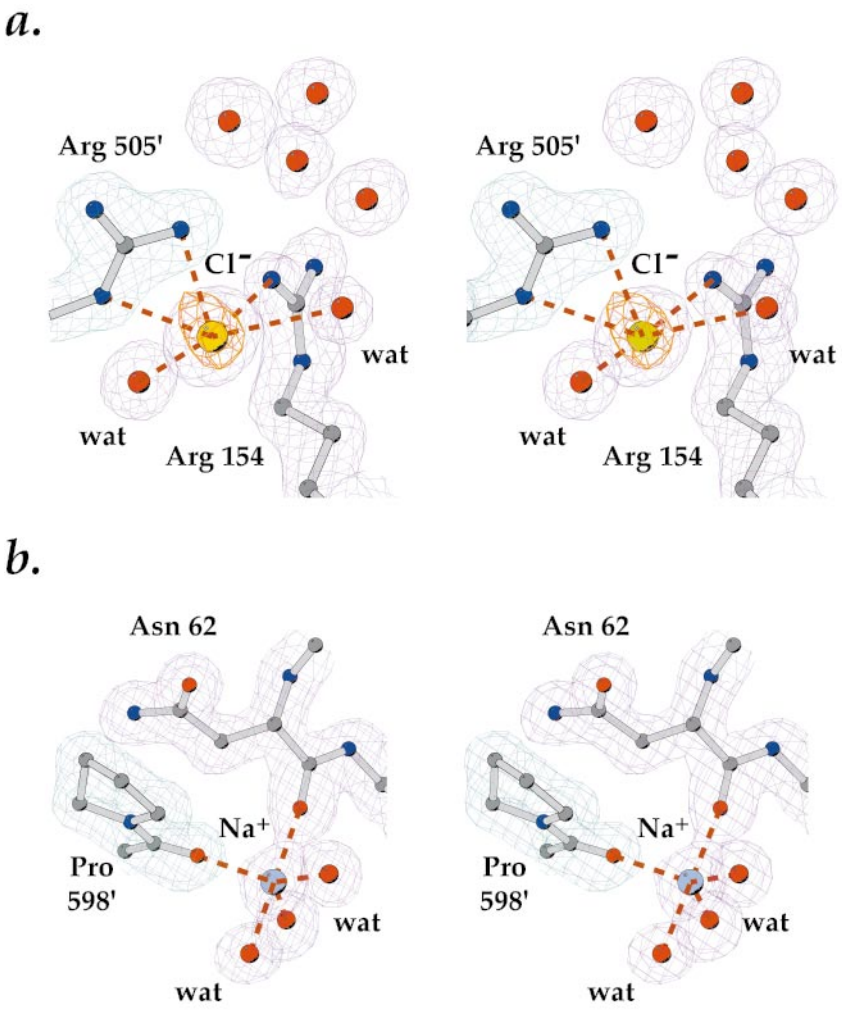

Figure 1. Stereo diagram of representative SIGMAA weighted $2F_o - F_c$ electron density maps of wild-type structure. Maps, contoured at 1.2σ, were computed using data to 1.62 Å resolution and phases from the refined model. Blue and green contours distinguish two different molecules related by crystallographic symmetry; primes distinguish labels of the second molecule. (a) The major site of chloride (yellow sphere) coordination reveals interactions with the guanidinium groups of Arg154 and Arg505′. Anomalous difference Fourier electron density for chloride is shown (computed with data between 2.4 Å to 50 Å resolution) as an orange map contoured at 4.5σ. (b) The major site of intermolecular sodium ion (cyan sphere) coordination reveals trigonal bipyramidal interactions with the carbonyl oxygen atoms of Asn62 and Pro598′. Figures 1, 2, 3(a), and 5 were generated by use of MOLSCRIPT[58] and BOBSCRIPT[59,60] and rendered with Raster3D.[61]

mined. The refined structures of PE reliably delineate specific interactions which might play a role in triggering the pH-induced conformational transition (Figure 2(d) and Table 1). In the polypeptide segment preceding the furin cleavage site, we see salt bridges between residues of domain II and counterparts in domain Ia, specifically His275-Glu80, Arg274-Asp139 (bridged by an interstitial H_2O molecule), as well as Glu270-Lys114. It is notable that the side-chains of the latter pair of

Table 1. Donor/acceptor interactions and solvent-accessible surface areas of amino acid side-chains that are candidates for involvement in the low pH-induced conformational change of PE

Residue	SC[a] accessible area (Å²)	Acceptor	Residue	SC[a] accessible area (Å²)	Donor	Distance (Å)
Glu80	13.5	$O^{\varepsilon 1}$	His275	7.9	$N^{\delta 1}$	3.0
Asp139	17.1	$O^{\delta 2}$	Arg274	6.9	NH1	2.8, 2.9[b]
Glu270	3.9	$O^{\varepsilon 2}$	Lys114	0.0	N_ζ	2.7
Asp366	4.9	$O^{\delta 1}$	His249	6.6	$N^{\delta 1}$	3.0
Asp366	4.9	$O^{\delta 2}$	Arg247	4.3	N^{ε}, NH2	2.7, 3.2
Asp384	14.9	$O_{\delta 1}$	Thr89	1.5	$O^{\gamma 1}$	2.9
Asp387	18.6	$O^{\delta 2}$	Arg247	4.3	NH2	2.8
Glu391	0.9	$O^{\varepsilon 2}$	His262	6.2	$N^{\varepsilon 2}$	2.5
Glu391	0.9	$O^{\varepsilon 2}$	Gln263	5.7	$N^{\varepsilon 2}$	2.8
Glu391	0.9	$O^{\varepsilon 1}$	Asn393	11.0	$N^{\delta 2}$	3.0

[a] SC, side-chain.
[b] Water-mediated contact; distances are between water molecule oxygen and acceptor/donor, respectively.

residues are almost completely solvent-inaccessible (Table 1); protonation of Glu270 would leave the (presumably) positively charged amino group of the lysine side-chain buried in the protein interior. Somewhat more remote from the furin site is a cluster of interactions between Glu391 of domain Ib and both His262 and Gln263 of domain II; in this cluster, the side-chain of Glu391 is also solvent-inaccessible. One can imagine plausible scenarios in which lowering the pH to ~5 would alter the protonation state of one partner in some or all of these salt bridges between domain II and domain I, resulting in, at a minimum, an ''untethering'' of the furin-susceptible segment of polypeptide from the surface of the molecule, and possibly in a more global disruption of the domain I - domain II interface.

An additional contribution to a pH-dependent conformational change may arise from the destabilization of the interface between domain Ia and Ib at their juncture with domain II. Studies have identified His246, Arg247 and His249 as amino acid residues whose collective mutagenesis to glutamic acid or glycine reduces toxicity on 3T3 cells, whereas mutagenesis of all three residues to lysine, which would retain a positive charge for each of them, does not impair toxicity.[39] These residues, along with Thr89, participate in a cluster of salt bridges and hydrogen bonds with three aspartic acid residues in domain Ib, specifically Asp366, Asp384, and Asp387. (Although His246 does not have a direct ion-pairing partner, its imidazole moiety is 5.7 Å from the carboxyl group of Glu270, and may contribute to perturbing the local electrostatic environment of the carboxyl group of this residue, which forms a salt bridge with Lys114.) Participation of these residues in the intoxication process argues in favor of a global conformational change preceding furin cleavage, rather than only a localized change around the protease target site, in view of their remoteness from the cleavage site.

In order to asses whether particular residues can be predicted to dominate the low pH-induced destabilization of the structure, we have computed the theoretical change in reaction field energy that would result from protonation of the carboxyl groups of individual aspartic and glutamic residues, using the finite difference Poisson-Boltzman method as described in Materials and Methods. Representative results for the wild-type structure are shown in Figure 3; similar results were obtained with parallel calculations using the coordinates of the mutant protein. The results shown in Figure 3 are notable for their lack of clear outliers from the general trend; there is no single residue at the interface between domains I and II which, when protonated, induces an unusually large change in calculated reaction field energy for the structure. (Of parenthetical interest, it is notable that the cluster of glutamic acid residues near to and including the catalytically essential Glu553 show the largest positive predicted change in reaction field energy when protonated.) Similar calculations in which the imidazole groups of individual histidine residues were protonated did not reveal any residues with unusually large positive energy changes (data not shown). Many of the positively charged groups which are solvent-inaccessible in the structure, such as the amino group of Lys114, are in relatively polar (albeit buried) environments, which may serve to stabilize the charge if the counterion of the ion pair is neutralized.

In summary, although there are several sets of ionic interaction which, when disrupted by protonation of one moiety, might contribute to the destabilization of the PA toxin structure, computational analysis suggests that no specific interaction dominates the process; destabilization may be dependent on multiple contributions from the concerted disruption of a network of ionic interactions. Further computational analysis of this process is underway (T.R. & P.K., unpublished results).

The furin cleavage site

In order to function as a sequence-specific endoprotease, furin must recognize an extended unstructured substrate. The consensus sequence for substrate recognition spans at least four residues amino-terminal to the scissile bond, and is given by the consensus sequence R_{P4}-X_{P3}-$(R/K)_{P2}$-R_{P1}-(scissile bond)-$X_{P1'}$, where arginine is essential at P1, and at least two of three amino acid residues at P2, P4, or P6 must be basic. Furthermore, the P1′ position should be neither hydrophobic nor aliphatic.[40]

The furin cleavage site of PE protrudes from the surface of domain II and is well ordered due to fortification with numerous main-chain and side-chain hydrogen bond interactions, as well as the Cys265-Cys287 disulfide (Figure 4(a)). Trp281 lies close to the cleavage site in the P2′ position; one face of the indole ring packs snugly against the side-chains of Leu267 and Thr271 of the helix preceeding the furin loop and Leu284 of the helix following the loop; the other face is completely solvent-exposed (Figure 4). The structure of the site in the W281A mutant shows no major differences from wild-type; the rms difference in coordinates of the polypeptide backbone between mutant and wild-type from residue 266 to 286 is 0.38 Å. However, there is a notable difference in the refined *B*-factors between the mutant and wild-type models; comparison of average main-chain *B*-factors (where restriction to main-chain atoms circumvents artifactual discrepancies due to side-chain disorder) reveals that the region where the mutant *B*-factors exceed those of wild-type by the largest positive value (which is to say, the region of greatest static disorder in the mutant relative to wild-type) is precisely at the cleavage site, with a value of ~16 $Å^2$ at Arg279 (Figure 5). This is in

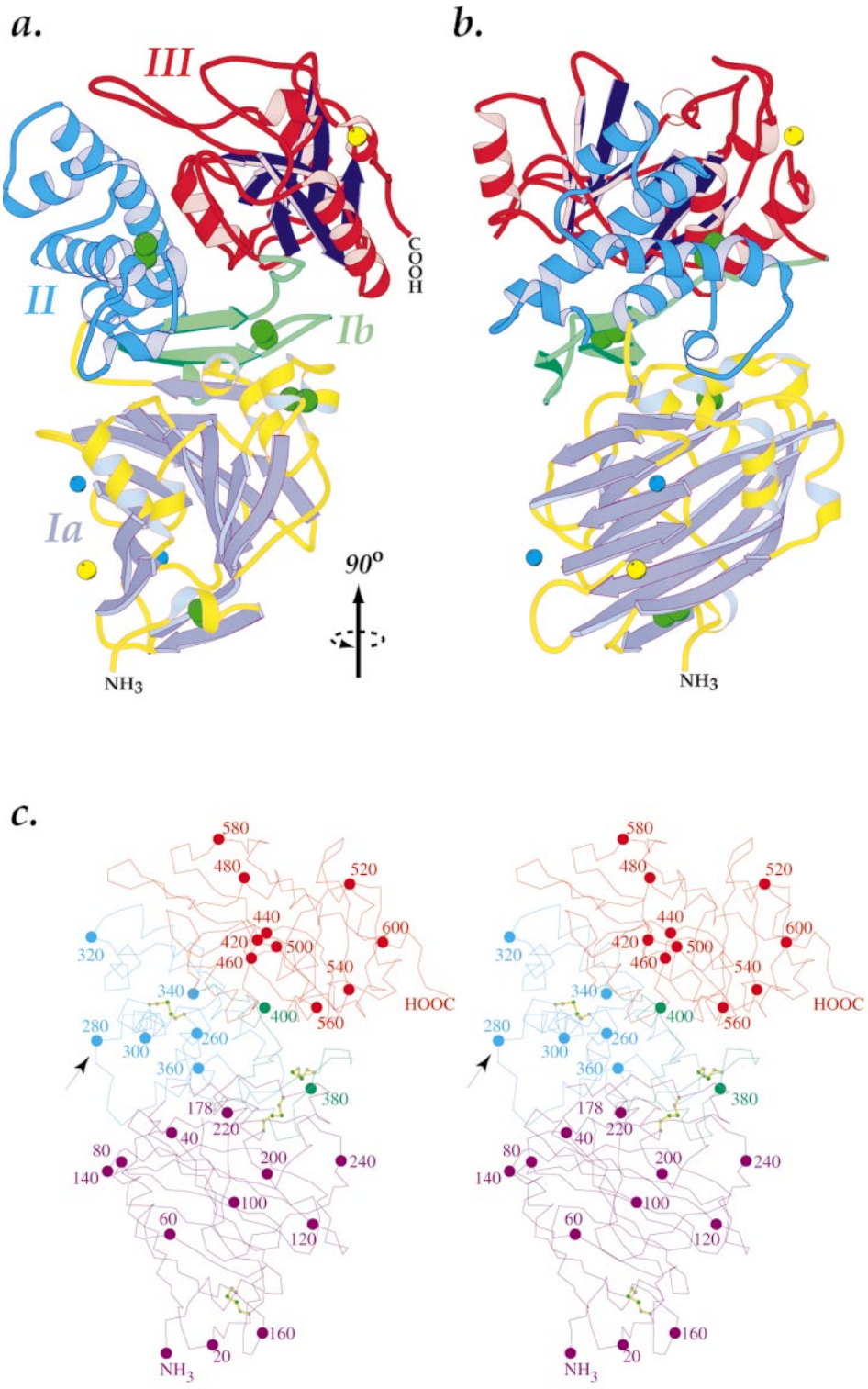

Figure 2(a)-(c) (*legend opposite*)

contrast to the general trend in differences between the two structures, where the average main-chain difference (mutant minus wild-type) is −5.0 Å^2, and most of the larger differences are found in segments of polypeptide on the surface of the molecule that are more poorly ordered in the wild-type model than in the mutant.

Although this information is derived from neutral-pH structures of PE, and cannot be rigorously extrapolated to pH 5, where the molecule is sus-

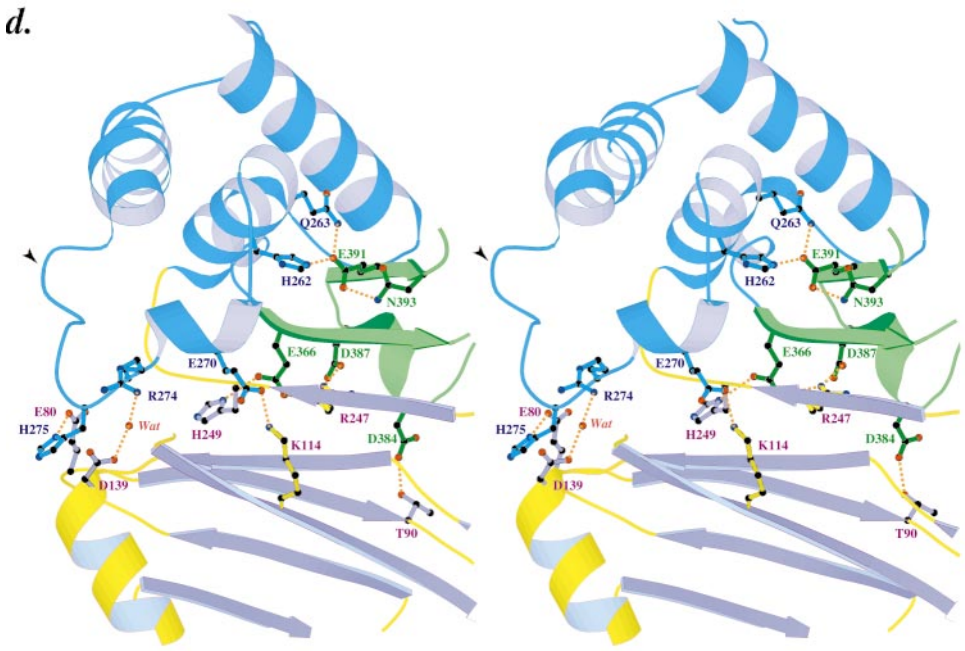

Figure 2. PE and the domain I - domain II interface. (a) Ribbon drawing of the tri-partite domain organization: domain Ia (1-252), purple β-sheet, yellow α-helices and coils; domain Ib (365-404), green β-sheet and coil; domain II (253-364), light blue β-sheet and coil; and domain III (405-613), red α-helix and coil, blue β-sheet. Cyan CPK spheres represent Na ions; yellow CPK spheres represent Cl ions; disulfide positions are indicated as green spheres. (b) Ribbon drawing rotated 90° from orientation in (a). (c) Stereographic C^{α} representation. Spherical main-chain atom positions are numbered every 20 amino acid residues. Color scheme and orientation based on (a). Disulfide positions are indicated as ball-and-stick side-chains. An arrow indicates the site of furin cleavage. (d) Stereographic representation of the ionic (salt-bridge) interactions at the interface between domains I and II. Broken lines indicate potential ionic interactions between side-chains that are likely to be disrupted under acidic conditions (shown in Table 1). An arrowhead indicates the site of furin cleavage. The orientation and color scheme are similar to that of (a).

ceptible to furin cleavage, it suggests that the W281A mutation may enhance the susceptibility of PE to furin through greater flexibility of the cleavage site, rather than through structural distortion. Information on the furin cleavage sites of other toxins is consistent with this suggestion. The robustness of the protease target site in the PE structure is in contrast to those of diphtheria toxin,[22] *E. coli* heat-labile toxin[41] and the anthrax protective antigen,[42] whose cleavage sites are disordered in the crystals, presumably due to flexibility. Systematic mutagenesis of the sequence of the cleavage site in PE toward that of diphtheria toxin revealed that replacement of residues 273-282 with their counterpart amino acids from diphtheria toxin (Figure 4(b)) resulted in essentially 100 % cleavage by furin at pH 5.5, in contrast to the 50 % observed with the wild-type sequence.[33] This replacement introduced glycine residues at positions 274 and 282, and replaced the tryptophan residue at 281 with valine; arguably, these changes would be anticipated to make the cleavage site more flexible. Along with these data, the structural comparison of the W281A mutant PE structure with wild-type favor the suggestion that flexibility of the furin cleavage site is an obligatory feature for efficient cleavage.

Ironically, although the W281A mutation makes the site substantially more susceptible to furin cleavage,[43] it reduces toxicity of the PE molecule. Additionally, mutation of Leu284 or Tyr289, as well as Trp281, substantially reduces toxicity of PE, despite (in some cases) enhancing susceptibility to furin cleavage.[43] Conservation of these specific residues near the cleavage site is apparently mandated by another step in the intoxication process, possibly interaction with an as yet unidentified intracellular component required for toxicity.

The enzymatic domain: activation and activity

Prior to activation, PE is devoid of ADP ribosyl transferase and NAD^+-glycohydrolase activities and does not bind NAD^+. The refined structures of PE in its proenzyme form helps to clarify the molecular constraints that impair catalytic activity. Independent structures of the enzymatically active domain III alone have been solved with ligands (i) β-methylene-thiazole-4-carboxyamide adenine dinucleotide, an NAD^+ analog (PDB accession code 1AER), giving a structure that mimics the substrate-bound state,[21] and (ii) AMP plus nicotinamide (PDB accession code 1DMA), giving a structure that mimics the product-bound state.[20] When compared to the earlier model of PE (in

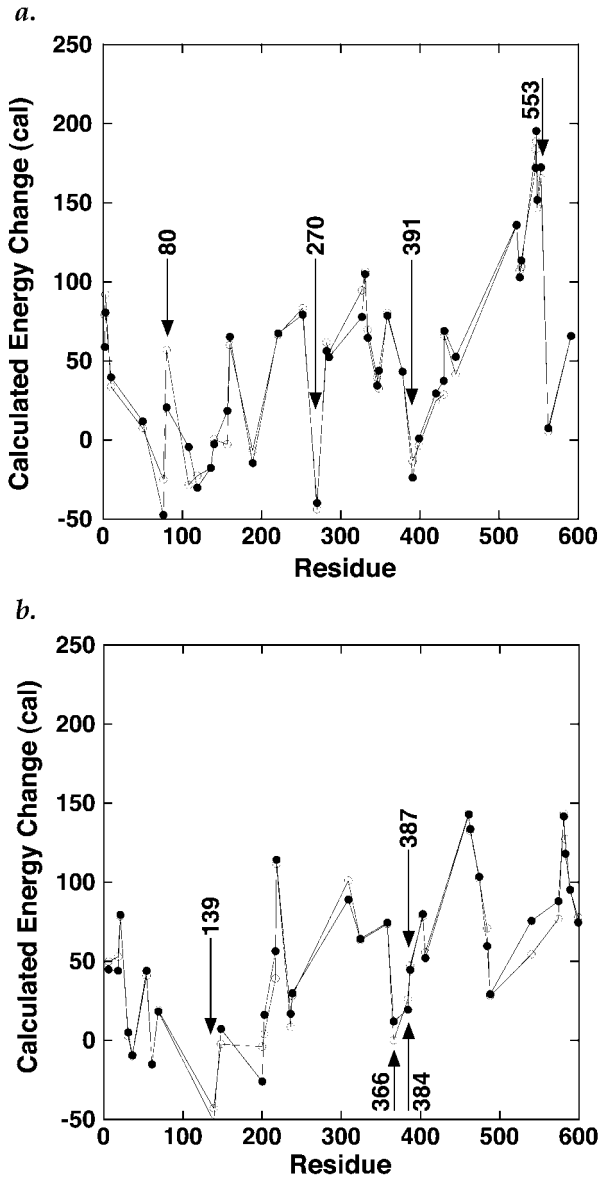

Figure 3. Calculated change in reaction field energy resulting from protonation of carboxyl groups of individual residues in the PA structure. (a) Glutamic acid residues: filled circles, protonation of OE1; open circles, protonation of OE2. Residues at the interface between domains I and II (shown in Figure 2(d)) are marked with arrows; the catalytic residue Glu553 is also marked. (b) Aspartic acid residues. Filled circles, protonation of OD1; open circles, protonation of OD2. Lines between points are included for visual clarification.

which two segments of polypeptide, designated L3 and L4 below, were absent from domain III[16]), these structures revealed that there are no global conformational differences between the active and proenzyme forms of the enzymatic domain. At the same time, they revealed a localized difference in a ''flexible loop'' that traverses the catalytic cleft, residues 458-463.

The refined model of PE elaborates the differences described earlier and also reveals others that were not clearly defined by comparisons to the earlier PE structure (Figure 6(a)). The ''flexible loop'' (L1; average rms displacement 4.1 Å) appears to be the primary determinant of inhibition; it is in an ''open'' conformation in the enzymatically active domain III structures, while in full-length PE, it is ''closed'' in a manner that sterically blocks NAD^+ binding. Ala457 and Ala464 act as swivel points for the loop. In PE, the well-ordered, closed conformation of L3 is stabilized by a helix from domain II, and most notably, by the side-chain of Arg467, which runs under the loop and forms a salt bridge with Glu348 of domain II. NAD^+ cannot bind until this interaction is disrupted; in PE, the backbone of residues 458-462 and side-chains of Arg458, Gln460 and Leu462 sterically block access of the ribose of the adenosine moiety and the diphosphate to the active site cleft.

Two other loops at the periphery of the substrate binding cleft show alternative conformations in PE and the domain III structures. These are designated L2, residues 517-522, and L3, residues 546-551 (Figure 6(a)). Inspection of crystal packing verifies that these differences cannot be ascribed to differences in intermolecular contacts. Although these loops are not in direct contact with bound substrate or product analogs in the structures of domain III, the conformational variations of these apparently flexible loops may result from indirect effects of ligand binding. In this context, it is notable that a W466F mutation reduces ADP ribosyl transferase activity 20-fold and glycohydrolase activity threefold.[44] This residue does not interact directly with substrate or product in structures of domain III; however, the side-chain of Trp466 interacts with Ala519 of L2. The W466F mutation may be propagating its effect indirectly by distorting the overall conformation of the substrate binding cleft, rather than by direct interaction with substrate.

Finally, loop L4, residues 486-493, which is very poorly ordered in all structures, shows significant conformational variability, not only between PE and domain III structures, but also between the wild-type and W281A mutant structures. The functional role of this loop has not been defined at this time.

During the later stages of refinement, well-defined electron density for a seven-atom molecule appeared in $F_o - F_c$ maps in the active site cleft of the W281A PE structure (Figure 6(b)). It approximately overlaps the bound nicotinamide molecule of one of the domain III structures (molecule B of PDB 1DMA), and the density can be ''filled'' with a carboxyl or carboxyamide group plus a four-atom chain, such as valeric acid or valeramide (with a carboxyamide group mimicking that of nicotinamide). The terminal atom on the extended chain of this molecule is ~2.3 Å from a carboxyl oxygen atom of the catalytic residue Glu553; however, $2F_o - F_c$ maps do not show continuous den-

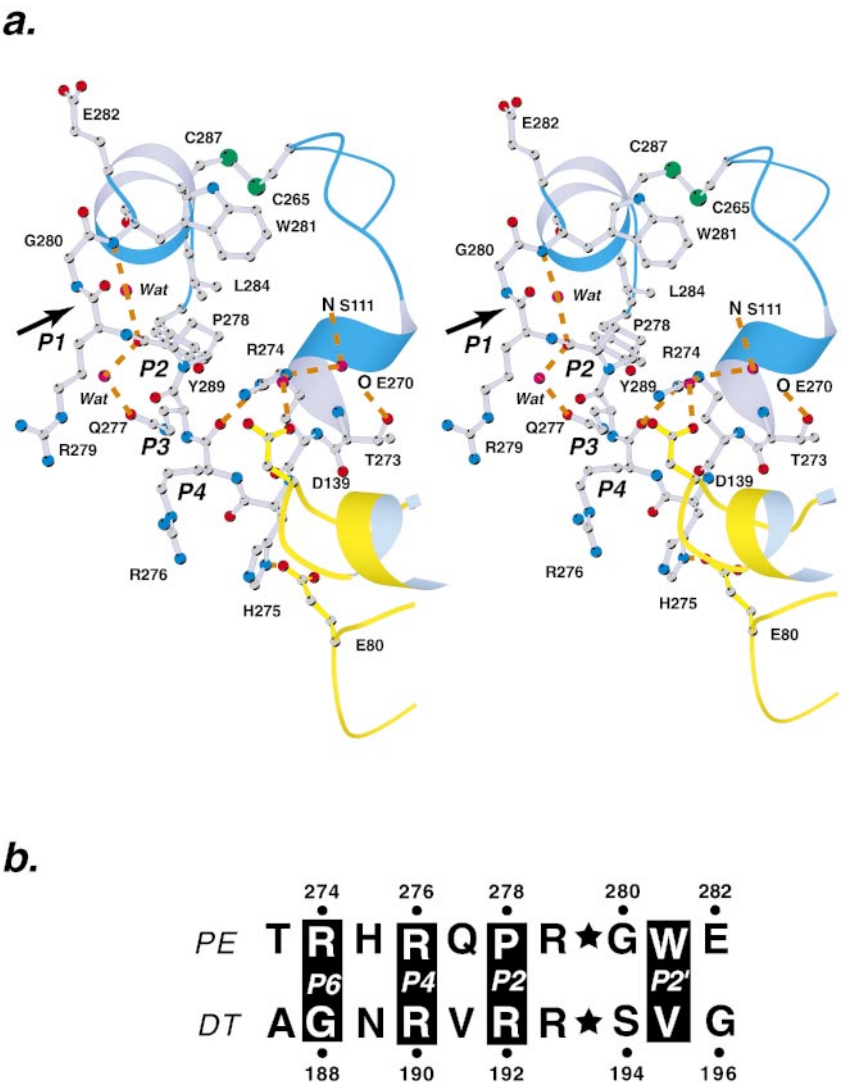

Figure 4. The furin cleavage site of PE. (a) Schematic stereo ribbon representation with selected amino acid residues depicted as ball-and-stick models. Side-chains that would bind to the P1-P4 sites of furin are labeled; an arrow indicates the site of cleavage. Broken lines indicate hydrogen bond or ionic interactions. The color scheme and molecular orientation are identical to those in Figure 1(a). (b) Sequence alignment of the PE furin cleavage site with that of diphtheria toxin (DT). A star (★) indicates the site of peptide bond cleavage.

sity between these atoms, so the ligand is not covalently linked to Glu553. The appearance of a non-substrate small molecule bound to the active site cleft of the enzymatic domain is reminiscent of the binding of ApUp to diphtheria toxin;[45] we note in passing that efforts to bind ApUp to PE and to observe it crystallographically yielded negative results (data not shown). We have been unable to trace this molecule to any component in our crystallization or cryoprotection reagents; hence, although it is well-ordered and presumably tightly bound, both its origin and its identity remain a mystery.

Receptor binding

Studies have identified Lys57 as a residue whose replacement with glutamic acid reduces PE toxicity toward 3T3 cells by two orders of magnitude, apparently by impairing receptor binding.[46] Additionally, insertion of a dipeptide between residues 60 and 61 reduces toxicity affinity by 500-fold.[47] These data provide circumstantial identification of the receptor binding region of PE on a concave surface of domain I. The structure of a receptor binding domain of α_2-macroglobulin has been solved.[48,49] The fold is an eight-stranded antiparallel β jellyroll topology, reminiscent of the more complex 13-stranded jellyroll of domain Ia from PE. Superficially, one might suspect that these two domains would share a common receptor binding surface. However, the receptor binding region of the α_2-macroglobulin receptor binding domain maps primarily to an α-helix that forms a convex surface protruding from the eight-stranded fold. Hence, we cannot identify a structurally equivalent feature in domain I of PE. Therefore, despite their common jellyroll fold, the respective PE and α_2-macroglobulin receptor binding domains appear to bind the α_2-macroglobulin receptor in different manners.

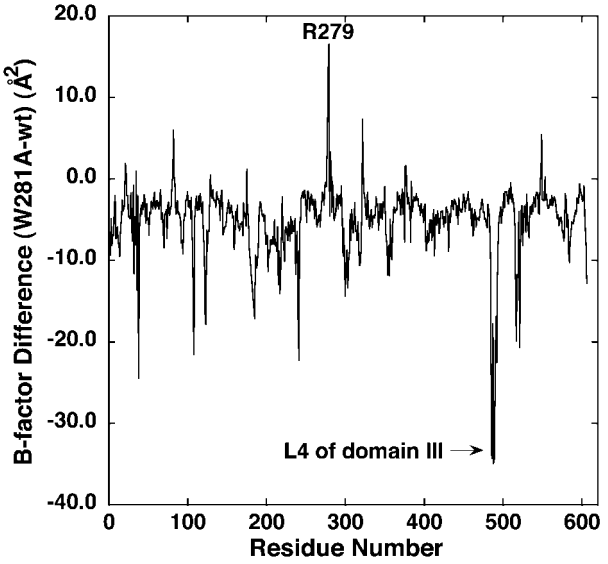

Figure 5. Difference in average main-chain *B*-factors between the W281A mutant and wild-type models. Largest positive (W281A more disordered than wild-type) and negative (wild-type more disordered than W281A) differences, at R281 and L4 (residues 486-493) respectively, are highlighted.

Summary

The refined high-resolution structure of PE reveals details of the molecular structure and intramolecular interactions that were ambiguous in earlier models. Specific interactions between domains I and II that may regulate the pH-dependent conformational change of PE have been delineated. The structure displays a well-ordered furin cleavage site, which contrasts with DT and the anthrax protective antigen; the combination of substantial differences in *B*-factors and minimal differences in static structure of the furin site between wild-type and the W281A mutant structures suggest that flexibility, rather than a specific tertiary structure, may regulate cleavage susceptibility. The refined PE structure also illustrates the molecular constraints that restrain the enzymatic domain in a non-catalytic state in full-length PE. The precision of the current models should facilitate the design and interpretation of further experiments on the molecular mechanisms of PE intoxication.

Materials and Methods

Crystals

Purified wild-type and W281A mutant PE proteins were prepared in the laboratories of R.J.C. and D.F., respectively, and crystallized as described,[32] with substitution of 0.05 to 0.1 M K-Hepps (pH 8.0) for phosphate buffer. Crystals were stabilized in a mother liquor consisting of 20% (w/v) PEG 8000, 1.0 M NaCl, and 0.05 to 0.1 M K-Hepps (pH 8.0). For cryoprotection, wild-type PE crystals were adapted to mother liquor plus 20% PEG-400, and W281A crystals were adapted to mother liquor plus 15% (v/v) ethylene glycol; in both case, the adaptation was carried out stepwise, with 5% increments of cryoprotectant at 15 minute intervals, at 4 °C. Crystals were then captured in thin rayon loops and flash-frozen in a stream of nitrogen gas at ~100 K for data collection. Freezing reduced the volume of the unit cell by approximately 4% from its room temperature value (Table 2).

X-ray data collection

Data for crystals of wild-type PE were collected both on beamline 7-1 of the Stanford Synchrotron Radiation Laboratory (SSRL) with an MAR Research image plate detector, and in-house on an R-AXIS IIC image plate detector system (Rigaku/MSC) using graphite monochromatized CuK_α radiation, since we were unable to complete re-collection of overloaded synchrotron data at the time (Table 1). In both cases, reflection intensities were integrated and scaled, and Lorentz-polarization corrections were applied with DENZO and SCALEPACK.[50] Although no special effort was made for in-house data collection to collect the anomalous diffraction signal, the favorable orientation of the crystal allowed ~84.4% of I^+ and 91.2% of I^- reflections to be recorded. Bijvoet mates were treated independently in data reduction. The two datasets were merged in order to compensate for the significant fraction of reflections that were discarded as overloaded in the synchrotron data. This was accomplished through local scaling of synchrotron data to in-house data with the program HEAVY v4.5[51] using 27,864 common reflections ($F/\sigma(F) > 0$) between 10 and 2.25 Å resolution. Then, the two datasets were combined using in-house data in the resolution range 50.0-2.40 Å and synchrotron data in the range 2.40-1.62 Å. The resulting dataset is 95.4% complete overall.

Data were collected on a crystal of W281A PE on SSRL beamline 9-2 using an ADSC CCD detector. Data were collected in two passes, the first using a 30 second exposure for 0.5° oscillations to optimize signal-to-noise at the higher resolution, and the second using a three second exposure to minimize overloads at lower resolution. Data were processed and scaled with DENZO and SCALEPACK.[50] Statistics are summarized in Table 1.

Structure determination and refinement

Model building was effected with the program O.[52,53] Model refinement was completed with the program package CNS version 1.0.[34] Superposition and comparison of models was done with LSQMAN of the Uppsala Software.[54]

The starting model for refinement of wild-type PE was derived from the atomic coordinates of the 3.0 Å structure;[16] 8% of the reflections were randomly removed to provide a cross-validation data set.[55] Throughout the refinement an overall anisotropic *B*-factor correction was applied to the data; final values for the tensor were: $B_{11} = -5.49$, $B_{22} = 2.82$, $B_{33} = 2.67$. Metal-ligand distances and geometry were not restrained in the refinement. In the first step, temperature factors were set to 24 Å^2 based upon a Wilson plot for all data to 2.25 Å resolution. Several segments of polypeptide

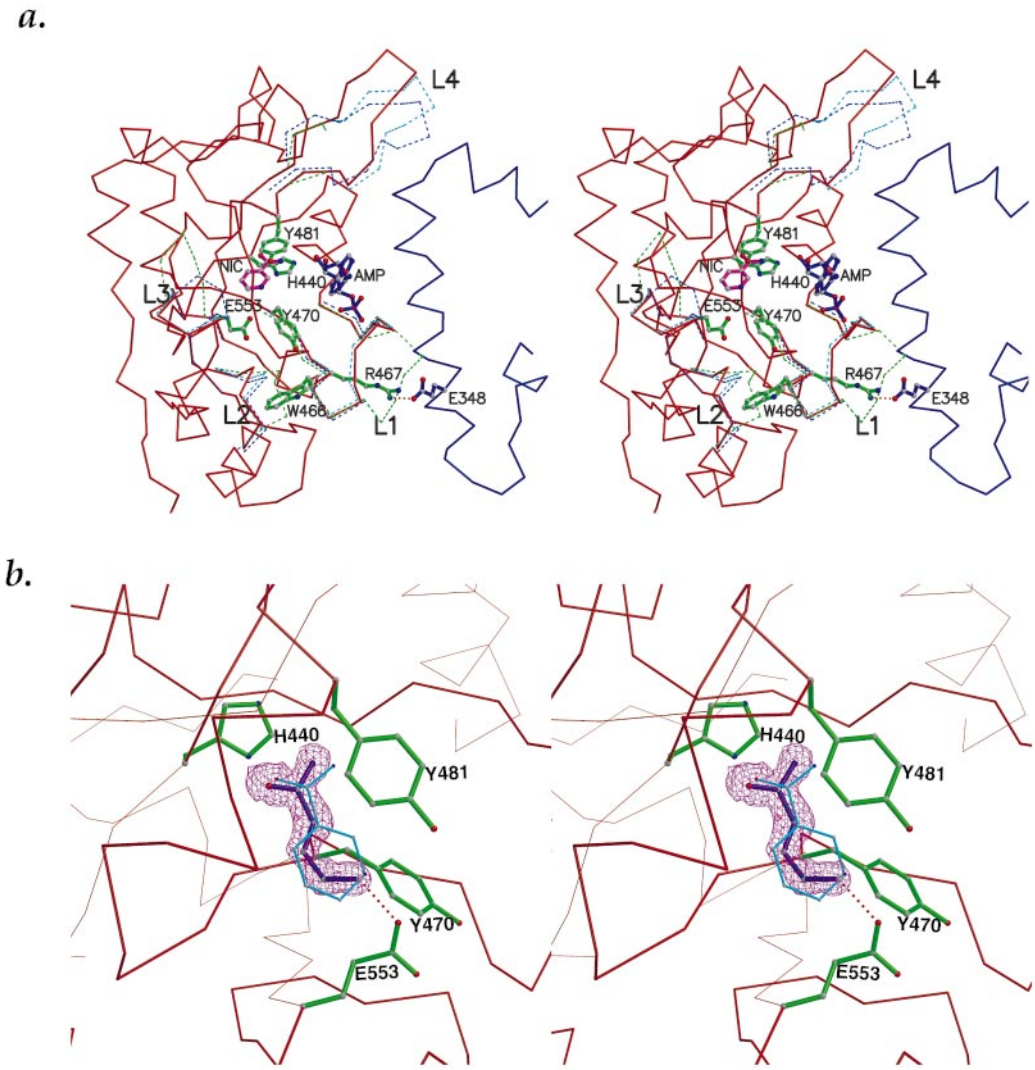

Figure 6. Conformational changes and ligand binding in the enzymatic domain (domain III) of PE. (a) Conformational changes in the C^{α} backbone of domain III. Continuous lines: C^{α} backbone of wild-type structure; blue, domain II; red, domain III. Dotted lines: C^{α} backbone traces in segments where they differ significantly from the wild-type model (L1, residues 458-463; L2, 517-522; L3, 546-551; L4, 486-493) when the respective domains III are superimposed. Color scheme: cyan, W281A mutant of PE; blue, molecule A of enzymatic domain alone; green, molecule B of enzymatic domain; both enzymatic domain structures are from PDB 1DMA.[20] Several amino acid side-chains relevant to ADP-ribosyl transferase activity (green), as well as the AMP (blue) and nicotinamide (magenta) molecules associated with molecule B of PDB 1DMA, are depicted as ball-and-stick models. (b) $F_o - F_c$ electron density map revealing a small molecule bound to domain III of W281A mutant PE. Map (magenta), computed using data to 1.45 Å resolution and phases from the refined model, is contoured at 4.5σ. C^{α} backbone trace of W281A PE is shown in red; selected side-chains are shown in green. A seven-atom molecule (dark blue) is modeled into the density; the nicotinamide molecule from coordinates 1DMA[20] is shown in cyan for comparison.

were omitted from the initial model, including residues 483-491, 548-551 and 604-613. Rigid body refinement was performed using data between 15 and 4 Å, then extended sequentially to 3.0 Å and 2.4 Å. The inclusion of low-resolution data was accompanied by use of a bulk solvent correction, calculated after each round of positional refinement. Rigid body refinement gave $R_{cryst} = 0.388$ ($R_{free} = 0.385$) for all data between 50 Å and 2.4 Å resolution. The model was then subjected to positional refinement, first to 2.7 Å resolution, then 2.4 Å resolution. Cartesian simulated annealing with a starting temperature of 3000° was applied prior to re-building, reducing the R_{cryst} to 0.269 ($R_{free} = 0.322$) to 2.4 Å resolution.

Successive cycles of manual fitting, followed by positional and restrained individual *B*-factor refinement, were carried out with extension of resolution to 2.4, 2.1, 1.8 and 1.62 Å. with manual rebuilding of the model into $2F_o - F_c$ and $F_o - F_c$ electron density maps computed with SIGMAA coefficients at each step. Regions derived from the original unrefined 3.0 Å model that required substantial manual rebuilding include residues

Table 2. Crystallographic data collection and refinement statistics

	Wild-type	W281A
A. *Space group and unit cell*		
Space group	$P2_1$	$P2_1$
a (Å)	59.5	59.9
b (Å)	98.1	99.1
c (Å)	58.3	58.6
β (deg.)	97.3	97.3
B. *Data collection*		
Wavelength (Å)	A: 1.54	
	B: 1.08	1.00
Resolution range (last shell) (Å)	A: 50.0-2.25 (2.37-2.25)	
	B: 20.0-1.62 (1.71-1.62)	60.0-1.40 (1.42-1.40)
Observations (total/unique)	A: 70,885/31,190	
	B: 224,879/80,328	293,233/116,635
Completeness (%)	A: 99.0 (97.0)	
	B: 93.0 (91.0)	88.2 (58.0)
Average I/σ	A: 32 (13)	
	B: 18 (6)	23.4 (5.8)
R_{sym}[a]	A: 0.028 (0.073)	
	B: 0.040 (0.185)	0.031 (0.117)
C. *Refinement*		
Resolution range (last shell) (Å)	50.0-1.62 (1.69-1.62)	60.0-1.45 (1.52-1.45)
R_{cryst}[b]	0.209 (0.286)	0.205 (0.270)
R_{free}	0.235 (0.320)	0.228 (0.299)
Number of reflections (working set)	73,810	97,274
Number of reflections (test set)	6477	10,852
Number of protein atoms	4637	4660
Number of solvent/hetero atoms	546/4 (2 Cl^-, 2 Na^+)	542/4 (2 Cl^-, 2 Na^+)
Residues absent from final model	1; 179-184; 607-613	1; 179-184; 607-613
Residues whose side-chains have two alternate conformations	R74, M129, V175, N215, E221, I239, L342	S65, R74, N207, R293, V308, T517, E522
Average *B* value, main chain (Å^2)	24.0	19.0
Average *B* value, all atoms (Å^2)	29.5	21.9
rmsd bond length (Å)	0.006	0.008
rmsd angles (deg.)	1.40	1.40

[a] $R_{sym} = \Sigma|I_{hkl} - \langle I_{hkl}\rangle|/\Sigma\langle I_{hkl}\rangle$, where I_{hkl} = single value of measured intensity of *hkl* reflection, and $\langle I\rangle$ = mean of all measured value intensity of *hkl* reflection.

[b] $R_{cryst} = \Sigma|F_{obs} - F_{calc}|/\Sigma F_{obs}$, where F_{obs} = observed structure factor amplitude and F_{calc} = structure factor calculated from model. R_{free} is computed in the same manner as R_{cryst}, using the test set of reflections.

8-10, 31-39, 104-108, 120-126, 178-192, 301-302, 317-322, 353-355, 485-492, and 517-520. At a resolution of 1.8 Å, two alternate conformations, each with 50 % occupancy, were added for the side-chains of residues Arg74, Met129, Val175, Asp215, Glu221, Ile239 and Leu342. Two Na ions and two Cl ions were identified based on their peak height in electron density maps and coordination geometry. Bijvoet differences from the in-house data were used to compute anomalous difference Fouriers to 2.4 Å; peaks in the resulting maps corroborated the assignment of the Cl ions and verified the positions of sulfur atoms in the model. Refinement and other vital statistics for the final model for wild-type PE are summarized in Table 1.

The W281A mutant structure was solved and refined with a similar strategy, using the refined wild-type model as a starting point. Initial rigid-body refinement with the wild-type PE polypeptide to 2.0 Å resolution gave $R_{cryst} = 0.333$ ($R_{free} = 0.334$); after torsional simulated annealing and energy minimization, manual rebuilding, and inclusion of solvent molecules, the statistics improved to $R_{cryst} = 0.227$ ($R_{free} = 0.249$). Resolution was then extended to 1.6 Å, with refinement and manual rebuilding, until statistics improved to $R_{cryst} = 0.220$ ($R_{free} = 0.238$), and subsequently to 1.45 Å. Final values for the anisotropic *B*-factor correction that was applied to the data are: $B_{11} = -2.60$, $B_{22} = 0.63$, $B_{33} = 1.97$. Modeling of several poorly ordered loops was verified with simulated annealing omit maps; additionally, the final model was verified with composite omit maps and compared with the wild-type structure for consistency. The ions from the wild-type structure were then included in the model, and residues which showed multiple conformations in $F_o - F_c$ maps were built with two conformations of equal occupancy. Refinement and other statistics are summarized in Table 1.

Computational analysis

The theoretical change in reaction field energy resulting from the protonation of individual residues was computed using the finite-difference Poisson-Boltzman method implemented in the program DelPhi.[56] Protons were built onto each selected side-chain using in-house software (P.K., unpublished results) that placed each hydrogen atom with proper distance and angle geometry and rotated the O-H group to avoid steric clashes with the rest of the protein. Two sets of calculations were performed, with the hydrogen atom built onto each of the

two carboxylic acid oxygen atoms. CHARMM22 charges and atomic radii were used for the DelPhi calculations.[57] The charges of the remaining residues and the amino and carboxy termini were maintained at their standard values at pH 7.0. The two Na and two Cl ions were included in the calculations, as was a single water molecule that mediates the salt bridge interaction between Asp139 and Arg274.

Protein Data Bank accession numbers

The coordinates of wild-type and W281A mutant PE have been deposited in the RCSB Protein Data Bank, accession numbers 1IKQ and 1IKP, respectively.

Note added in proof

DNA sequencing has recently identified a P201Q mutation in the coding sequence of the PA toxin gene in the expression plasmid for recombinant W281A mutant toxin (D.F., personal communication). We have confirmed the presence of the P201Q mutation in the W281 mutant protein used in this study by inspection of electron density maps. Residue 201 is ~35 Å from the furin cleavage site; conclusions regarding the W281A mutation are unlikely to be influenced by the P201Q mutation.

Acknowledgments

The authors thank Drs Marcelo Sousa and Sigurd Wilbanks for their assistance in collection of the synchrotron X-ray data. This work was supported by National Institutes of Health (NIH) grant GM-39928 to D.B.M., a Burroughs Wellcome Fund Fellowship of the Life Sciences Research Foundation (to J.E.W.), Damon Runyan Cancer Research Foundation fellowship DRG-1575 (to T.M.R.), and a Howard Hughes Medical Institute Predoctoral Fellowship and Stanford Graduate Fellowship (to M.D.). Portions of this research were carried out at the Stanford Synchrotron Radiation Laboratory, a national user facility operated by Stanford University on behalf of the US Department of Energy, Office of Basic Energy Sciences. The SSRL Structural Molecular Biology Program is supported by the Department of Energy, Office of Biological and Environmental Research, and by the National Institutes of Health, National Center for Research Resources, Biomedical Technology Program, and the National Institute of General Medical Sciences.

References

1. Cromer, D. T. (1974). Dispersion corrections for X-ray atomic scattering factors. In *International Tables for X-ray Crystallography (Revised and Supplementary Tables to Volumes II and III)* (Ibers, J. A. & Hamilton, W. C., eds), pp. 149-153, The Kynoch Press, Birmingham, UK.
2. Frank, D. W. & Iglewski, B. H. (1988). Kinetics of toxA and regA mRNA accumulation in *Pseudomonas aeruginosa*. *J. Bacteriol.* **170**, 4477-4483.
3. Van Ness, B. G., Howard, J. B. & Bodley, J. W. (1980). ADP-ribosylation of elongation factor 2 by diphtheria toxin. Isolation and properties of the novel ribosyl-amino acid and its hydrolysis products. *J. Biol. Chem.* **255**, 10717-10720.
4. Moehring, J. M. & Moehring, T. J. (1988). The post-translational trimethylation of diphthamide studied *in vitro*. *J. Biol. Chem.* **263**, 3840-3844.
5. Perentesis, J. P., Miller, S. P. & Bodley, J. W. (1992). Protein toxin inhibitors of protein synthesis. *Biofactors,* **3**, 173-184.
6. Kounnas, M. Z., Morris, R. E., Thompson, M. R., FitzGerald, D. J., Strickland, D. K. & Saelinger, C. B. (1992). The alpha 2-macroglobulin receptor/low density lipoprotein receptor-related protein binds and internalizes *Pseudomonas* exotoxin A. *J. Biol. Chem.* **267**, 12420-12423.
7. Chiron, M. F., Fryling, C. M. & FitzGerald, D. J. (1994). Cleavage of *Pseudomonas* exotoxin and diphtheria toxin by a furin-like enzyme prepared from beef liver. *J. Biol. Chem.* **269**, 18167-18176.
8. Inocencio, N. M., Moehring, J. M. & Moehring, T. J. (1994). Furin activates *Pseudomonas* exotoxin A by specific cleavage *in vivo* and *in vitro*. *J. Biol. Chem.* **269**, 31831-31835.
9. Corboy, M. J. & Draper, R. K. (1997). Elevation of vacuolar pH inhibits the cytotoxic activity of furin-cleaved exotoxin A. *Infect. Immun.* **65**, 2240-2242.
10. Ogata, M., Chaudhary, V. K., Pastan, I. & FitzGerald, D. J. (1990). Processing of *Pseudomonas* exotoxin by a cellular protease results in the generation of a 37,000-Da toxin fragment that is translocated to the cytosol. *J. Biol. Chem.* **265**, 20678-20685.
11. Hessler, J. L. & Kreitman, R. J. (1997). An early step in *Pseudomonas* exotoxin action is removal of the terminal lysine residue, which allows binding to the KDEL receptor. *Biochemistry,* **36**, 14577-14582.
12. Chaudhary, V. K., Jinno, Y., FitzGerald, D. & Pastan, I. (1990). *Pseudomonas* exotoxin contains a specific sequence at the carboxyl terminus that is required for cytotoxicity. *Proc. Natl Acad. Sci. USA,* **87**, 308-312.
13. Hazes, B. & Read, R. J. (1997). Accumulating evidence suggests that several AB-toxins subvert the endoplasmic reticulum-associated protein degradation pathway to enter target cells. *Biochemistry,* **36**, 11051-11054.
14. Lord, J. M. & Roberts, L. M. (1998). Toxin entry: retrograde transport through the secretory pathway. *J. Cell Biol.* **140**, 733-736.
15. McKee, M. L. & FitzGerald, D. J. (1999). Reduction of furin-nicked *Pseudomonas* exotoxin A: an unfolding story. *Biochemistry,* **38**, 16507-16513.
16. Allured, V. S., Collier, R. J., Carroll, S. F. & McKay, D. B. (1986). Structure of exotoxin A of *Pseudomonas aeruginosa* at 3.0-Angstrom resolution. *Proc. Natl Acad. Sci. USA,* **83**, 1320-1324.
17. Guidi-Rontani, C. & Collier, R. J. (1987). Exotoxin A of *Pseudomonas aeruginosa*: evidence that domain I functions in receptor binding. *Mol. Microbiol.* **1**, 67-72.
18. Hwang, J., Fitzgerald, D. J., Adhya, S. & Pastan, I. (1987). Functional domains of *Pseudomonas* exotoxin identified by deletion analysis of the gene expressed in *E. coli*. *Cell,* **48**, 129-136.
19. Reiter, Y. & Pastan, I. (1998). Recombinant Fv immunotoxins and Fv fragments as novel agents for cancer therapy and diagnosis. *Trends Biotechnol.* **16**, 513-520.
20. Li, M., Dyda, F., Benhar, I., Pastan, I. & Davies, D. R. (1995). The crystal structure of *Pseudomonas aeruginosa* exotoxin domain III with nicotinamide and AMP: conformational differences with the intact exotoxin. *Proc. Natl Acad. Sci. USA,* **92**, 9308-9312.

21. Li, M., Dyda, F., Benhar, I., Pastan, I. & Davies, D. R. (1996). Crystal structure of the catalytic domain of *Pseudomonas* exotoxin A complexed with a nicotinamide adenine dinucleotide analog: implications for the activation process and for ADP ribosylation. *Proc. Natl Acad. Sci. USA,* **93**, 6902-6906.
22. Choe, S., Bennett, M. J., Fujii, G., Curmi, P. M., Kantardjieff, K. A., Collier, R. J. & Eisenberg, D. (1992). The crystal structure of diphtheria toxin. *Nature,* **357**, 216-222.
23. Sixma, T. K., Pronk, S. E., Kalk, K. H., Wartna, E. S., van, Z. B., Witholt, B. & Hol, W. G. (1991). Crystal structure of a cholera toxin-related heat-labile enterotoxin from *E. coli*. *Nature,* **351**, 371-377.
24. Stein, P. E., Boodhoo, A., Armstrong, G. D., Cockle, S. A., Klein, M. H. & Read, R. J. (1994). The crystal structure of pertussis toxin. *Structure,* **2**, 45-57.
25. Han, S., Arvai, A. S., Clancy, S. B. & Tainer, J. A. (2001). Crystal structure and novel recognition motif of rho ADP-ribosylating C3 exoenzyme from *Clostridium botulinum*: structural insights for recognition specificity and catalysis. *J. Mol. Biol.* **305**, 95-107.
26. Ruf, A., Mennissier de Murcia, J., de Murcia, G. M. & Schulz, G. E. (1996). Structure of the catalytic fragment of poly(AD-ribose) polymerase from chicken. *Proc. Natl Acad. Sci. USA,* **93**, 7481-7485.
27. Jiang, J. X., Abrams, F. S. & London, E. (1991). Folding changes in membrane-inserted diphtheria toxin that may play important roles in its translocation. *Biochemistry,* **30**, 3857-3864.
28. Silverman, J. A., Mindell, J. A., Zhan, H., Finkelstein, A. & Collier, R. J. (1994). Structure-function relationships in diphtheria toxin channels. I. Determining a minimal channel-forming domain. *J. Membr. Biol.* **137**, 17-28.
29. el Bayâ, A., Linnemann, R., von Olleschik-Elbheim, L., Robenek, H. & Schmidt, M. A. (1997). Endocytosis and retrograde transport of pertussis toxin to the Golgi complex as a prerequisite for cellular intoxication. *Eur. J. Cell Biol.* **73**, 40-48.
30. Lencer, W. I., Constable, C., Moe, S., Jobling, M. G., Webb, H. M., Ruston, S. *et al*. (1995). Targeting of cholera toxin and *Escherichia coli* heat labile toxin in polarized epithelia: role of COOH-terminal KDEL. *J. Cell Biol.* **131**, 951-962.
31. Jackson, M. E., Simpson, J. C., Girod, A., Pepperkok, R., Roberts, L. M. & Lord, J. M. (1999). The KDEL retrieval system is exploited by *Pseudomonas* exotoxin A, but not by Shiga-like toxin-1, during retrograde transport from the Golgi complex to the endoplasmic reticulum. *J. Cell Sci.* **112**, 467-475.
32. Collier, R. J. & McKay, D. B. (1982). Crystallization of Exotoxin A from *Pseudomonas aeruginosa*. *J. Mol. Biol.* **157**, 413-415.
33. Chiron, M. F., Ogata, M. & FitzGerald, D. J. (1996). *Pseudomonas* exotoxin exhibits increased sensitivity to furin when sequences at the cleavage site are mutated to resemble the arginine-rich loop of diphtheria toxin. *Mol. Microbiol.* **22**, 769-778.
34. Brünger, A. T., Adams, P. D., Clore, G. M., DeLano, W. L., Gros, P., Grosse-Kunstleve, R. W. *et al*. (1998). Crystallography & NMR system: a new software suite for macromolecular structure determination. *Acta Crystallog. sect. D,* **54**, 905-921.
35. Luzzati, V. (1952). Traitment statistique des erreurs dans la determination des structures cristallines. *Acta Crystallog.* **5**, 802-810.
36. Glusker, J. P. (1991). Structural aspects of metal liganding to functional groups in proteins. In *Advances in Protein Chemistry* (Anfinsen, C. B., Edsall, J. T., Richards, F. M. & Eisenberg, D. S., eds), vol. 42, pp. 1-76, Academic Press, Orlando.
37. Toney, M. D., Hohenester, E., Cowan, S. W. & Jansonius, J. N. (1993). Dialkylglycine decarboxylase structure: bifunctional active site and alkali metal sites. *Science,* **261**, 756-759.
38. Jiang, J. X. & London, E. (1990). Involvement of denaturation-like changes in *Pseudomonas* exotoxin A hydrophobicity and membrane penetration determined by characterization of pH and thermal transitions. Roles of two distinct conformationally altered states. *J. Biol. Chem.* **265**, 8636-8641.
39. Chaudhary, V. K., Jinno, Y., Gallo, M. G., FitzGerald, D. & Pastan, I. (1990). Mutagenesis of *Pseudomonas* exotoxin in identification of sequences responsible for the animal toxicity. *J. Biol. Chem.* **265**, 16306-16310.
40. Matthews, D. J., Goodman, L. J., Gorman, C. M. & Wells, J. A. (1994). A survey of furin substrate specificity using substrate phage display. *Protein Sci.* **3**, 1197-1205.
41. Sixma, T. K., Kalk, K. H., van, Z. B., Dauter, Z., Kingma, J., Witholt, B. & Hol, W. G. (1993). Refined structure of *Escherichia coli* heat-labile enterotoxin, a close relative of cholera toxin. *J. Mol. Biol.* **230**, 890-918.
42. Petosa, C., Collier, R. J., Klimpel, K. R., Leppla, S. H. & Liddington, R. C. (1997). Crystal structure of the anthrax toxin protective antigen. *Nature,* **385**, 833-838.
43. Zdanovsky, A. G., Chiron, M., Pastan, I. & FitzGerald, D. J. (1993). Mechanism of action of *Pseudomonas* exotoxin. Identification of a rate-limiting step. *J. Biol. Chem.* **268**, 21791-21799.
44. Beattie, B. K., Prentice, G. A. & Merrill, A. R. (1996). Investigation into the catalytic role for the tryptophan residues within domain III of *Pseudomonas aeruginosa* exotoxin A. *Biochemistry,* **35**, 15134-15142.
45. Barbieri, J. T., Carroll, S. F., Collier, R. J. & McCloskey, J. A. (1981). An endogenous dinucleotide bound to diphtheria toxin. Adenylyl-(3′,5′)-uridine 3′-monophosphate. *J. Biol. Chem.* **256**, 12247-12251.
46. Jinno, Y., Chaudhary, V. K., Kondo, T., Adhya, S., FitzGerald, D. J. & Pastan, I. (1988). Mutational analysis of domain I of *Pseudomonas* exotoxin. Mutations in domain I of *Pseudomonas* exotoxin which reduce cell binding and animal toxicity. *J. Biol. Chem.* **263**, 13203-13207.
47. Chaudry, G. J., Wilson, R. B., Draper, R. K. & Clowes, R. C. (1989). A dipeptide insertion in domain I of exotoxin A that impairs receptor binding. *J. Biol. Chem.* **264**, 15151-15156.
48. Jenner, L., Husted, L., Thirup, S., Sottrup-Jensen, L. & Nyborg, J. (1998). Crystal structure of the receptor-binding domain of alpha 2-macroglobulin. *Structure,* **6**, 595-604.
49. Huang, W., Dolmer, K., Liao, X. & Gettins, P. G. (2000). NMR solution structure of the receptor binding domain of human alpha(2)-macroglobulin. *J. Biol. Chem.* **275**, 1089-1094.
50. Otwinowski, Z. & Minor, W. (1997). Processing of X-ray diffraction data collected in oscillation mode. *Methods Enzymol.* **276**, 307-326.
51. Terwilliger, T. C., Kim, S.-H. & Eisenberg, D. (1987). Generalized method of determining heavy-atom positions using the difference Patterson function. *Acta Crystallog. sect. A,* **43**, 1-5.

52. Jones, T. A. (1978). A graphics model building and refinement system for macromolecules. *J. Appl. Crystallog.* **11**, 268-272.
53. Jones, T. A., Zhou, J. Y., Cowan, S. W. & Kjeldgaard, M. (1991). Improved methods for the muilding of protein models in electron density maps and the location of errors in these models. *Acta Crystallog. sect. A,* **47**, 110-119.
54. Kleywegt, G. J. & Jones, T. A. (1997). Detecting folding motifs and similarities in protein structures. *Methods Enzymol.* **277**, 525-545.
55. Brünger, A. T. (1992). The free *R* value: a novel statistical quantity for assessing the accuracy of crystal structures. *Nature,* **355**, 472-474.
56. MacKerell, A., Bashford, D., Bellott, M., Dunbrack, R., Evanseck, J., Field, M. *et al*. (1998). All-atom empirical potential for molecular modeling and dynamics studies of proteins. *J. Phys. Chem.* **B102**, 3586-3616.
57. Honig, B. & Nicholls, A. (1995). Classical electrostatics in biology and chemistry. *Science,* **268**, 1144-1149.
58. Kraulis, P. (1991). MOLSCRIPT: a program to produce both detailed and schematic plots of protein structures. *J. Appl. Crystallog.* **24**, 946-950.
59. Esnouf, R. M. (1997). An extensively modified version of MolScript that includes greatly enhanced coloring capabilities. *J. Mol. Graph. Model.* **15**, 132-134.
60. Esnouf, R. M. (1999). Further additions to MolScript version 1.4, including reading and contouring of electron-density maps. *Acta Crystallog. sect. D,* **55**, 938-940.
61. Merritt, E. A. & Bacon, D. J. (1997). Raster3D: photorealistic molecular graphics. *Methods Enzymol.* **277**, 505-524.

Edited by D. Rees

(Received 3 July 2001; received in revised form 17 October 2001; accepted 18 October 2001)